Editors' Suggestion   Featured in Physics

Experimental Characterization of Defect-Induced Phonon Lifetime Shortening

Boyao Liu[*], Jack Kelsall, David J. Ward, and Andrew P. Jardine

Cavendish Laboratory, University of Cambridge, 19 J J Thomson Avenue, Cambridge CB3 0HE, United Kingdom

We present the first direct experimental measurement of defect-induced lifetime shortening of acoustic surface phonons. Defects are found to contribute a temperature-independent component to the linewidths of Rayleigh wave phonons on a Ni(111) surface. We also characterized the increase in phonon scattering with both surface defect density and phonon wave vector. A quantitative estimate of the scattering rate between phonon modes and surface line defects is extracted from the experimental data for the first time.

Thermal management is a pressing issue in many fields of science and technology, but nowhere more so than in the fast moving microelectronics industry [1]. The development of high density electronic devices has brought huge advances in computational capability, in turn enabling huge societal benefits, but the intense levels of heat dissipation in such devices bring major challenges and ultimately limit performance [2,3]. New device architectures, e.g., based on 2D materials, are currently of great interest as they have the prospect to address these demands [4–7], as well as to lower overall power consumption [3]. Typically, phonons are the main heat carriers in all these devices [4,8–10]. Although phonon-phonon scattering events can influence thermal conductivity, in real materials, the thermal conductivity is usually limited by the presence of lattice imperfections or defects, including vacancies, interstitials, dislocations, and grain boundaries. Consequently, there have been great efforts to investigate defect interactions with phonons [11–17]. Most important in the present context is the influence of defects on acoustic phonon lifetimes, which determines the thermal conductivity [18,19]. However, acoustic phonon lifetime shortening induced by defects is extremely challenging to measure; direct experimental observation is still lacking, especially in 2D systems, and so far the issue has mainly been explored through theoretical calculations and computer simulations [20–26].

Here, we report the first direct measurement of the influence of crystal defects on acoustic phonon lifetime on a Ni(111) surface. We measure changes in the Rayleigh wave (RW) mode phonon linewidth (inversely proportional to lifetime) using helium spin echo (HeSE), while tuning the surface defect density. Although many techniques have been used to study phonons, they generally have limited energy resolution, or are limited by the $q = 0$ selection rule. By using HeSE, we can investigate specific phononic states in the dispersive regime with μeV energy resolution [27]. We show that the phonon lifetimes vary with momentum and decrease with surface defect density due to defect-phonon scattering, which enables us to make a quantitative estimate of coupling between the RW mode and surface defects.

Figure 1 shows a schematic of the HeSE instrument used to measure surface phonon spectra [27]. In brief, a beam of
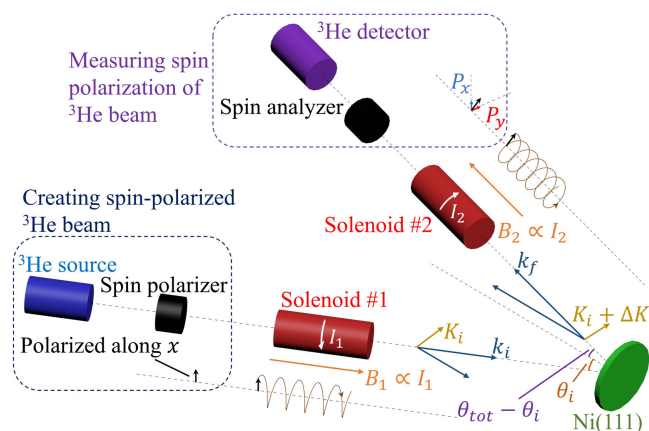

FIG. 1. Schematic representation of a HeSE phonon measurement. The ^{3}He beam is scattered from the Ni(111) sample surface, where dashed lines represent the trajectory of the beam and the surface normal. The total scattering angle, $\theta_{tot} = 44.4°$, is fixed; the sample can be rotated to change the incidence angle θ_i to investigate specific phononic states. k_i and k_f are the wave vectors of the incident and scattered ^{3}He atoms, with surface parallel components $K_i = k_i \sin\theta_i$ and $K_f = K_i + \Delta K = k_f \sin(\theta_{tot} - \theta_i)$, respectively. The ^{3}He beam is nuclear spin polarized along the x direction before entering the solenoids. In the two solenoids, the atoms undergo spin precession, as illustrated by the helices. The final beam polarization is measured along the two perpendicular directions, giving P_x and P_y.
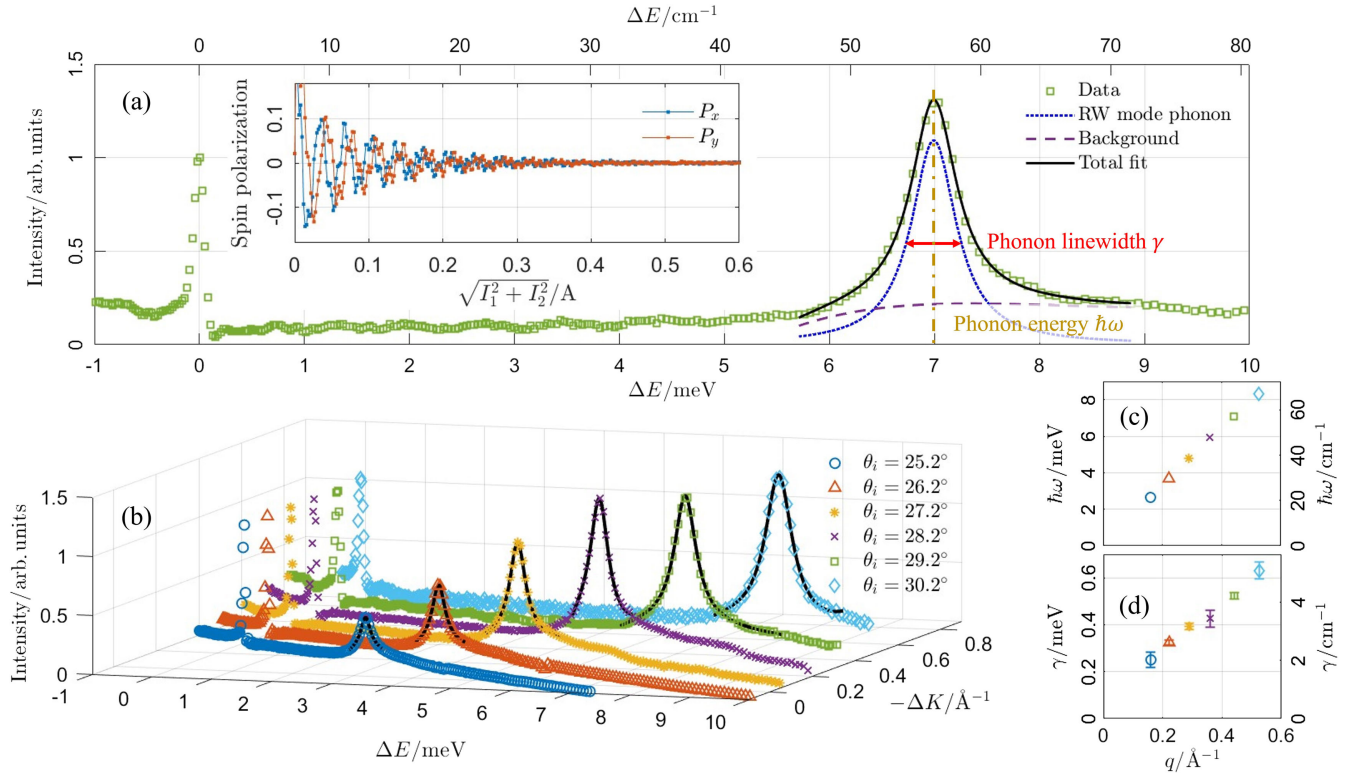
FIG. 2. (a) Typical HeSE energy transfer spectrum (green squares) obtained at an incident angle $\theta_i = 29.2°$. The blue dotted line is a Lorentzian function representing the RW phonon peak, while the purple dashed line is a quartic polynomial representing the background. The black solid line shows the sum of the two. The inset shows the raw spin polarization data as a function of the solenoid current magnitude $(I_1^2 + I_2^2)^{1/2}$, from which the energy transfer spectrum is obtained by Fourier transforming and scaling. (b) Energy transfer spectra for six different values of θ_i from 25.2° to 30.2°, in steps of 1° and including surface parallel momentum transfer, ΔK. Black lines represent the fits to the sum of a Lorentzian function and quartic polynomial. (c) Centers of the Lorentzian functions in (b), corresponding to the RW phonon energies, as a function of phonon wave vector or momentum transfer, q. (d) RW phonon linewidths, obtained from the FWHM of the Lorentzian functions, as a function of q. Error bars in this figure and the subsequent figures represent 95% confidence interval of the fitting process. All data are collected along the ΓM direction on a Ni(111) surface, with a ^{3}He beam energy of 8.07 meV, a surface temperature of 500 K, and a ^{3}He surface reflectivity of $R = 0.31$.

^{3}He atoms is generated by the ^{3}He source and is spin polarized in the x direction after passing through the spin polarizer. The polarized beam then passes through two solenoids, before and after scattering from the sample surface, in each of which the ^{3}He nuclear spins acquire a Larmor precession phase angle about the beam axis. The rate of spin precession in each solenoid is determined by the respective currents, denoted I_1 and I_2. Finally, the overall state of the beam is measured using the spin analyzer and detector to obtain the two polarization components, P_x and P_y. In each scan we measure (P_x, P_y) as we vary (I_1, I_2), with I_1/I_2 fixed. The polarization data can then be Fourier transformed and scaled to yield the spectrum of energy exchange ΔE of ^{3}He atoms with the surface. Phonons on the surface will result in a peak in the energy spectrum. By optimizing the ratio I_1/I_2 for the measurement, we can accurately resolve the line shape for any particular phononic state even if the energy spread of the incoming ^{3}He beam is finite (typically about 0.5 meV),

and $\alpha = \arctan(I_1/I_2)$ is known as the "tilt angle." Further details describing the method can be found in [31–33].

Figure 2(a) shows an example energy transfer spectrum within which an RW phonon feature is observed. The inset shows the measured polarization (P_x, P_y), as a function of the solenoid current magnitude, $(I_1^2 + I_2^2)^{1/2}$, from which the energy transfer spectrum, shown in the main figure, is obtained. To analyze the data, the phonon peak is assigned a Lorentzian profile, while the background, due to multiphonon scattering, etc., is represented by a quartic polynomial (results are insensitive to the exact form). The center of the peak gives the phonon energy $\hbar\omega$, while the FWHM of the peak gives its linewidth γ, represented by the red bar. In this work, by changing θ_i and α, six RW phononic states were studied, as shown in the Supplemental Material [28]. Examples of the energy transfer spectra taken from the same Ni(111) surface are shown in Fig. 2(b), together with the associated momentum change parallel to the surface, ΔK. Table I lists the values of θ_i and α for the experiments,

TABLE I. The incident angles and tilt angles used in the experiments shown in Figs. 2 and 3, together with the associated phonon energies and wave vectors. $\beta \approx \Delta\Gamma/\Delta n$ is the estimated proportionality constant between the defect-phonon scattering rate and surface line defect density.

Marker	$\theta_i/°$	$\alpha/°$	$\hbar\omega/\text{meV}$	$q/\text{Å}^{-1}$	$\beta/(\text{ps}^{-1}\,\text{Å})$
○	25.2	129.1	2.6	0.16	9.7
△	26.2	127.3	3.7	0.22	13.2
*	27.2	125.6	4.8	0.29	16.3
×	28.2	123.8	5.9	0.36	18.5
□	29.2	122.1	7.0	0.44	19.5
◇	30.2	120.5	8.3	0.53	19.7

together with phonon energies $\hbar\omega$ and phonon wave vectors q, extracted from the spectra. The dispersion of $\hbar\omega$ with q is also shown graphically in Fig. 2(c) and is in agreement with the literature [34–36]. RW phonon linewidths obtained from the six measurements are shown in Fig. 2(d), which increase with q, consistent with previous works on bulk materials using inelastic neutron scattering [9,37].

In our experiments, argon ion sputtering was used to create surface defects, while annealing was used to remove them [38]. The two methods were combined to control the surface defect density, which was then quantified by measuring the ^{3}He surface reflectivity R. Here, we define R as the number of specularly reflected helium atoms as a fraction of the number incident, measured when $\theta_i = \theta_{\text{tot}}/2 = 22.2°$ [28]. We prepared the Ni(111) surface by Ar$^+$ sputtering at 500 K and flash annealing to 800 K, followed by measuring R immediately afterward. The phonon spectra, illustrated in Fig. 2(c) and Table I, were taken in a randomized order; the corresponding linewidths were then extracted. Subsequently another short period of annealing was performed before the reflectivity and the phonon linewidths were measured again. Such cycles were repeated nine times, yielding the results in Figs. 3(a)–3(f), which show the mode linewidth as a function of reflectivity, each at different values of q.

For each of the phononic states, it is clear that the linewidth decreases as reflectivity rises, which we attribute to the reducing number of surface defects from which the phonons can scatter. The relationship is linear until $R \sim 0.42$, after which there is a small deviation as the reflectivities become very high. Fitting a linear model,

$$\gamma = -p_1 R + p_2, \tag{1}$$

to the linewidth variation across the first six data points of each phononic state, i.e., when $R < 0.42$, gives coefficients p_1, that characterize the rate of change of the linewidth, as shown in Fig. 3(g). We find that p_1 rises with q and ω, which means that phonons with higher energies experience a greater increase in linewidth broadening from the same

increase in surface defects. One possible qualitative explanation is that, since the penetration depth of a Rayleigh wave is comparable to the wave length, phonons with larger q are more localized on the surface, and thus experience more scattering from surface defects [39].

Previous works have demonstrated that after Ar$^+$ sputtering, surfaces are predominantly occupied by line defects such as step edges [38,40,41], and theoretical models have suggested that $p_1 \propto q^4$ for surface line defects [23]. However, our experiments show that p_1 is at first approximately proportional to q, and then the rate of increase drops as q exceeds $\sim 0.3\,\text{Å}^{-1}$. Similarly, the variation cannot be explained by other forms of defects in [23]. The disagreement indicates that the defects created by sputtering cannot be described by the arguments in [23], which treat defects as atoms with excess mass. Therefore, more sophisticated models are required.

Moreover, the defect-induced phonon linewidth broadening $\Delta\gamma$ is related to the increase in defect-phonon scattering rate $\Delta\Gamma$, by $\Delta\gamma = \hbar\Delta\Gamma$. $\Delta\Gamma$ should be proportional to the change in density of surface defects Δn (here n has the unit of reciprocal length because it is the length of line defects per unit area) [23,42]. We can use the data to estimate the rate of increase of phonon-defect scattering with defect density, which we denote $\beta(q)$. Since the value of R is high and given that helium is highly sensitive to surface defects, defect density n should be relatively low, such that the defects are well separated. Under these conditions the reflectivity can be written as [43]

$$R = R_0(1 - Dn), \tag{2}$$

where R_0 is the reflectivity of the sample when no defects exist; in this work we estimate it to be 0.6. D is the scattering cross section for line defects, which was determined to be $\sim 10\,\text{Å}$ in most cases [44–49]. Combining Eqs. (1) and (2), we arrive at

$$\beta(q) = \frac{\Delta\Gamma(q)}{\Delta n} = \frac{\Delta\gamma(q)}{\hbar\Delta n} = \frac{R_0 D}{\hbar}p_1(q) \approx \frac{6\,\text{Å}}{\hbar}p_1(q). \tag{3}$$

Calculated values of $\beta(q)$ are given in Table I. Both R_0 and D can be estimated to a precision of $\sim 30\%$, which suggests that overall, our calculation of $\beta(q)$ is accurate to about 50%.

When $R \gtrsim 0.42$, γ approaches a constant value. It suggests that annealing at $R \gtrsim 0.42$ can still remove surface defects and improve reflectivity, but scattering of phonons from surface line defects has become insignificant, and phonon-phonon scattering dominates the lifetime. This can be attributed to the high sensitivity of reflectivity measurement to other forms of surface defect, which may still be present in small numbers even at these exceptionally high reflectivity measurements. Such features could include vacancies or contaminants resulting from the finite sample
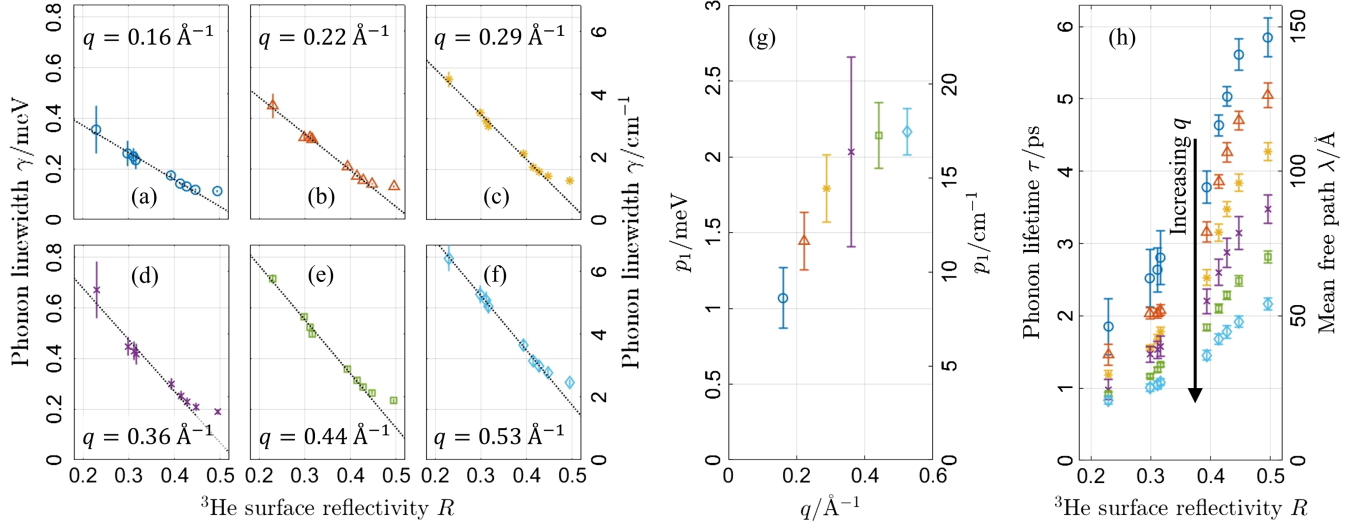
FIG. 3. (a)–(f) RW phonon linewidths as a function of ^{3}He surface reflectivity. Each marker type represents a certain phonon state, whose energy and momentum are shown in Table I and Fig. 2(c). Dotted lines represent the best fit of the first six data points to $\gamma = -p_1 R + p_2$. (g) The fitted parameters p_1 as a function of phonon wave vectors. (h) Phonon lifetimes τ determined from the data in (a)–(f) using $\tau = \hbar/\gamma$. Mean free paths λ are evaluated using $\lambda = v\tau$, where v is given in Eq. (4). Both decrease monotonically with increasing q. All the data correspond to the ΓM azimuth of a Ni(111) surface at 500 K.

purity. At lower reflectivities, such features would be masked by the cross section overlap with the much larger numbers of line defects induced by sputtering. This effect does not affect the results at lower reflectivities, and could be further studied by integrating HeSE with other surface characterization techniques, such as scanning tunneling microscopy. Since reflectivity measurement cannot reveal the direction of line defects, introducing other characterization techniques will also enable us to investigate how the direction of line defects affects phonon-lifetime shortening. Moreover, it is also possible to use HeSE to study phonons in stepped surfaces, which will provide further insight into defect-phonon interactions [50].

Figure 3(h) shows phonon lifetimes calculated from the data in Figs. 3(a)–3(f) using $\tau = \hbar/\gamma$. The linear dispersion in Fig. 2(c) has also been used to evaluate the phonon group velocity

$$v = \frac{\partial\omega}{\partial q} \approx 2.5 \text{ km/s}, \quad (4)$$

enabling the mean free path, $\lambda = v\tau$, to be included. At all values of R, the lifetimes and mean free paths strictly decrease as a function of q, which validates the agreement with previous works [9,37].

Finally, the temperature dependence of the phonon linewidth was studied. The reflectivity of the Ni(111) surface was tuned to $R = 0.31$ by sputtering and annealing. Afterward a series of energy transfer spectra was taken at various surface temperatures to obtain the RW phonon linewidths shown in Fig. 4 (upper line). The linewidths increase as a function of temperature, due to expected

phonon-phonon scattering that results from lattice anharmonicity [16,51–55]. The Ni crystal was further sputtered and annealed until R reached 0.45. The same phonon linewidth measurements were repeated, giving the additional set of results shown in Fig. 4 (lower line). The effect of increasing R is a temperature-independent drop in phonon linewidth, in agreement with previous works on
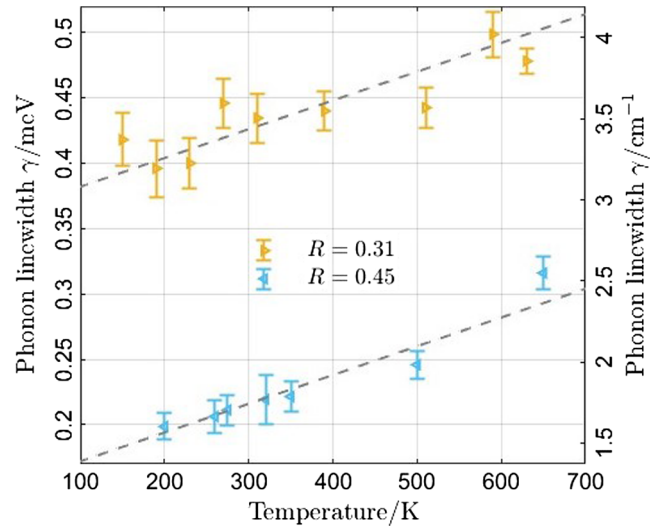

FIG. 4. Temperature dependence of defect-induced linewidth broadening. Linewidths are shown for a particular phononic state ($q = 0.47$ Å^{-1} along the direction 6° away from the ΓK azimuth, and $\hbar\omega = 7$ meV) at various temperatures and two different values of reflectivity of 0.31 and 0.45. Gray dashed lines provide a guide to the eye, showing a shifted, but otherwise identical temperature dependence at different reflectivities.

optical phonons [13,14,16] and our interpretation of temperature-independent defect scattering.

In summary, we have presented the first extensive characterization of the influence of surface defects on acoustic phonon lifetimes. We showed that, on a Ni(111) surface, the presence of defects adds a temperature-independent component to phonon linewidth γ. By controlling the number of surface defects using Ar^+ sputtering and annealing, we showed that phonon linewidths decrease linearly as reflectivity increases, due to a reduced rate of defect-phonon scattering. We managed to obtain a characteristic q dependence that is inconsistent with existing models in the literature, and thus motivates the need for new theories. Since these reflectivity changes are known to be predominantly due to line defects, we were able to estimate the change in the rate of phonon scattering with line defect density, $\beta(q) = \Delta\Gamma(q)/\Delta n$, given in Table I. We are not aware of any prior experimental measurements for the scattering strength in this fundamental phonon-defect interaction.

One of the important benefits of our approach is that it can easily be generalized to other systems and other types of defects, and that it has the ability to resolve linewidths of phonons at all crystal orientations. It enables us to examine defect-phonon scattering processes, and thus to engineer thermal characteristics in various systems. We anticipate the method being particularly valuable for 2D materials, which are candidates for next-generation transistors and thermoelectric devices [3,6,56] and where thermal properties are often the limiting factor in improving overall performance [1]. Since defects are inevitably, and often deliberately, introduced during doping and other fabrication processes, the ability to examine the interplay between defects and phonons has the potential to help develop new electronic technology that will change our lives in the upcoming decades.

The supporting data for this Letter are openly available from [57].

---

[*]bl476@cam.ac.uk

[1] A. L. Moore and L. Shi, Emerging challenges and materials for thermal management of electronics, Mater. Today **17**, 163 (2014).

[2] J. Zou and A. Balandin, Phonon heat conduction in a semiconductor nanowire, J. Appl. Phys. **89**, 2932 (2001).

[3] M. Chhowalla, D. Jena, and H. Zhang, Two-dimensional semiconductors for transistors, Nat. Rev. Mater. **1**, 16052 (2016).

[4] X. Xu, J. Chen, and B. Li, Phonon thermal conduction in novel 2D materials, J. Phys. Condens. Matter **28**, 483001 (2016).

[5] C. Tan, X. Cao, X.-J. Wu, Q. He, J. Yang, X. Zhang, J. Chen, W. Zhao, S. Han, G.-H. Nam, M. Sindoro, and H. Zhang, Recent advances in ultrathin two-dimensional nanomaterials, Chem. Rev. **117**, 6225 (2017).

[6] H. Song, J. Liu, B. Liu, J. Wu, H.-M. Cheng, and F. Kang, Two-dimensional materials for thermal management applications, Joule **2**, 442 (2018).

[7] X. Zhang, S. Yin, L. Bao, Q. Wang, J. Liang, L. Guo, H. Xue, Y. Huang, H. Zhu, C. Wan, and W. Fu, MoS_2/organics superlattices for surface-enhanced supra-Nernstian biochemical detection, Cell Rep. Phys. Sci. **4**, 101575 (2023).

[8] Z. Zhou, X. Yang, H. Fu, R. Wang, X. Lu, G. Wang, and X. Zhou, Anomalous thermal transport driven by electron–phonon coupling in 2D semiconductor h-BP, Adv. Funct. Mater. **32**, 2206974 (2022).

[9] A. Gold-Parker, P. M. Gehring, J. M. Skelton, I. C. Smith, D. Parshall, J. M. Frost, H. I. Karunadasa, A. Walsh, and M. F. Toney, Acoustic phonon lifetimes limit thermal transport in methylammonium lead iodide, Proc. Natl. Acad. Sci. U.S.A. **115**, 11905 (2018).

[10] M. Songvilay, M. Bari, Z.-G. Ye, G. Xu, P. M. Gehring, W. D. Ratcliff, K. Schmalzl, F. Bourdarot, B. Roessli, and C. Stock, Lifetime-shortened acoustic phonons and static order at the Brillouin zone boundary in the organic-inorganic perovskite $CH_3NH_3PbCl_3$, Phys. Rev. Mater. **2**, 123601 (2018).

[11] X. Yan, C. Liu, C. A. Gadre, L. Gu, T. Aoki, T. C. Lovejoy, N. Dellby, O. L. Krivanek, D. G. Schlom, R. Wu, and X. Pan, Single-defect phonons imaged by electron microscopy, Nature (London) **589**, 65 (2021).

[12] C. A. Gadre, X. Yan, Q. Song, J. Li, L. Gu, H. Huyan, T. Aoki, S. W. Lee, G. Chen, R. Wu, and X. Pan, Nanoscale imaging of phonon dynamics by electron microscopy, Nature (London) **606**, 292 (2022).

[13] Y. Wang, H. Dai, Z. Liu, and D. Liu, Phonon scattering in monolayer molybdenum disulfide under different defect concentrations based on temperature-dependent Raman spectra, J. Phys. Chem. C **127**, 1109 (2023).

[14] B. Eckert, R. Bini, H. J. Jodl, and S. Califano, High resolution infrared spectra of the ν_3 vibron in natural sulfur and in the isotopically pure ^{32}S crystal, J. Chem. Phys. **100**, 912 (1994).

[15] M. Zhao, W. Pan, C. Wan, Z. Qu, Z. Li, and J. Yang, Defect engineering in development of low thermal conductivity materials: A review, J. Eur. Ceram. Soc. **37**, 1 (2017).

[16] R. Cuscó, J. H. Edgar, S. Liu, J. Li, and L. Artús, Isotopic disorder: The prevailing mechanism in limiting the phonon lifetime in hexagonal BN, Phys. Rev. Lett. **124**, 167402 (2020).

[17] C. L. Wan, W. Pan, Q. Xu, Y. X. Qin, J. D. Wang, Z. X. Qu, and M. H. Fang, Effect of point defects on the thermal transport properties of $(La_xGd_{1-x})_2Zr_2O_7$: Experiment and theoretical model, Phys. Rev. B **74**, 144109 (2006).

[18] P. Klemens, Heat conduction in solids by phonons, Thermochim. Acta **218**, 247 (1993).

[19] A. A. Taleb and D. Farías, Phonon dynamics of graphene on metals, J. Phys. Condens. Matter **28**, 103005 (2016).

[20] Z. Yan, M. Yoon, and S. Kumar, Influence of defects and doping on phonon transport properties of monolayer MoSe$_2$, 2D Mater. **5**, 031008 (2018).

[21] M. B. Bebek, C. M. Stanley, T. M. Gibbons, and S. K. Estreicher, Temperature dependence of phonon-defect interactions: Phonon scattering vs phonon trapping, Sci. Rep. **6**, 32150 (2016).

[22] B. Mortazavi and S. Ahzi, Thermal conductivity and tensile response of defective graphene: A molecular dynamics study, Carbon **63**, 460 (2013).

[23] R. G. Steg and P. G. Klemens, Scattering of Rayleigh waves by surface defects, J. Appl. Phys. **45**, 23 (1974).

[24] S. K. Estreicher, T. M. Gibbons, and M. B. Bebek, Thermal phonons and defects in semiconductors: The physical reason why defects reduce heat flow, and how to control it, J. Appl. Phys. **117**, 112801 (2015).

[25] T. Held, I. Pfeiffer, and W. Kuhn, Influence of isotopic disorder on phonon frequencies and phonon linewidths of an anharmonic crystal, Phys. Rev. B **55**, 231 (1997).

[26] R. Guo and S. Lee, Mie scattering of phonons by point defects in IV-VI semiconductors PbTe and GeTe, Mater. Today Phys. **12**, 100177 (2020).

[27] A. Jardine, H. Hedgeland, G. Alexandrowicz, W. Allison, and J. Ellis, Helium-3 spin-echo: Principles and application to dynamics at surfaces, Prog. Surf. Sci. **84**, 323 (2009).

[28] See Supplemental Material at http://link.aps.org/supplemental/10.1103/PhysRevLett.132.056202, which includes Refs. [29,30] for the phononic states studied in this work, the methods of controlling and characterizing surface defect density, phonon spectra at various temperatures, and the influence of adsorbates on phonon measurements.

[29] J. Manson, Chapter 3 energy transfer to phonons in atom and molecule collisions with surfaces, in *Dynamics, Handbook of Surface Science* Vol. 3, edited by E. Hasselbrink and B. Lundqvist (North-Holland, Amsterdam, 2008), pp. 53–93.

[30] H. Dorothy, S. Bawa, and John H. Thomas, III, *Handbook of Vacuum Science and Technology.* (Academic Press, New York, 1998).

[31] G. Alexandrowicz, Helium spin echo spectroscopy: Measuring the dynamics of atoms, molecules and surfaces, Ph.D. thesis, University of Cambridge, Cambridge, UK, 2005.

[32] P. R. Kole, A. P. Jardine, H. Hedgeland, and G. Alexandrowicz, Measuring surface phonons with a ^{3}He spin echo spectrometer: A two-dimensional approach, J. Phys. Condens. Matter **22**, 304018 (2010).

[33] G. Alexandrowicz and A. P. Jardine, Helium spin-echo spectroscopy: Studying surface dynamics with ultra-high-energy resolution, J. Phys. Condens. Matter **19**, 305001 (2007).

[34] W. Menezes, P. Knipp, G. Tisdale, and S. J. Sibener, Surface phonon spectroscopy of Ni(111) studied by inelastic electron scattering, Phys. Rev. B **41**, 5648 (1990).

[35] A. al Taleb, G. Anemone, D. Farías, and R. Miranda, Acoustic surface phonons of graphene on Ni(111), Carbon **99**, 416 (2016).

[36] A. Tamtögl, E. Bahn, J. Zhu, P. Fouquet, J. Ellis, and W. Allison, Graphene on Ni(111): Electronic corrugation and dynamics from helium atom scattering, J. Phys. Chem. C **119**, 25983 (2015).

[37] P.-F. Lory *et al.*, Direct measurement of individual phonon lifetimes in the clathrate compound Ba$_{7.81}$Ge$_{40.67}$Au$_{5.33}$, Nat. Commun. **8**, 491 (2017).

[38] M. Ondrejcek, W. Swiech, I. Petrov, M. Rajappan, and C. P. Flynn, LEEM investigations of surfaces using a beam of energetic self-ions, Microsc. Res. Tech. **72**, 197 (2009).

[39] Y. M. Poplavko, Chapter 2—mechanical properties of solids, in *Electronic Materials*, edited by Y. M. Poplavko (Elsevier, New York, 2019), pp. 71–93.

[40] B. Poelsema, L. K. Verheij, and G. Comsa, "Two-layer" behavior of the Pt(111) surface during low-energy Ar$^+$-ion sputtering at high temperatures, Phys. Rev. Lett. **53**, 2500 (1984).

[41] A. M. Lahee, J. R. Manson, J. P. Toennies, and C. Wöll, Observation of interference oscillations in helium scattering from single surface defects, Phys. Rev. Lett. **57**, 471 (1986).

[42] R. G. Steg and P. G. Klemens, Scattering of Rayleigh waves by surface irregularities, Phys. Rev. Lett. **24**, 381 (1970).

[43] B. Poelsema and G. Comsa, *Scattering of Thermal Energy Atoms: From Disordered Surfaces* (Springer, New York, 2006), Vol. 115.

[44] L. K. Verheij, B. Poelsema, and G. Comsa, Investigation of a randomly stepped Pt(111) surface using thermal energy atom scattering (TEAS), Surf. Sci. **162**, 858 (1985).

[45] A. Sánchez and S. Ferrer, Cross section for diffuse scattering from random steps on Cu(100) determined by TEAS (thermal energy atom scattering), Surf. Sci. **187**, L587 (1987).

[46] M. Patting, D. Farías, and K. H. Rieder, Determination of step-edge orientation by helium atom scattering, Phys. Rev. B **62**, 2108 (2000).

[47] J. J. de Miguel, J. Camarero, and R. Miranda, Studies of surface diffusion and growth on Cu(111) by means of thermal energy atom scattering, J. Phys. Condens. Matter **14**, 6155 (2002).

[48] B. Poelsema, K. Lenz, and G. Comsa, The dissociative adsorption of hydrogen on Pt(111): Actuation and acceleration by atomic defects, J. Chem. Phys. **134**, 074703 (2011).

[49] D. Farias and K.-H. Rieder, Atomic beam diffraction from solid surfaces, Rep. Prog. Phys. **61**, 1575 (1998).

[50] L. Niu, D. J. Gaspar, and S. J. Sibener, Phonons localized at step edges: A route to understanding forces at extended surface defects, Science **268**, 847 (1995).

[51] G. Benedek and J. P. Toennies, Systematic trends in the normal enhancement of the phonon anharmonicity at the surface of metals, Phys. Rev. B **46**, 13643 (1992).

[52] G. Bracco, L. Bruschi, L. Pedemonte, and R. Tatarek, Anharmonic effects at the onset of the Ag(110) roughening transition, Surf. Sci. **352–354**, 964 (1996).

[53] A. P. Baddorf and E. W. Plummer, Enhanced surface anharmonicity observed in vibrations on Cu(110), Phys. Rev. Lett. **66**, 2770 (1991).

[54] K. Kern, U. Becher, P. Zeppenfeld, G. Comsa, B. Hall, and D. L. Mills, Anharmonic linewidth broadening of surface phonons, Chem. Phys. Lett. **167**, 362 (1990).

[55] D. S. Kim, O. Hellman, N. Shulumba, C. N. Saunders, J. Y. Y. Lin, H. L. Smith, J. E. Herriman, J. L. Niedziela, D. L. Abernathy, C. W. Li, and B. Fultz, Temperature-dependent phonon lifetimes and thermal conductivity of silicon by inelastic neutron scattering and *ab initio* calculations, Phys. Rev. B **102**, 174311 (2020).

[56] X.-L. Zhu, P.-F. Liu, J. Zhang, P. Zhang, W.-X. Zhou, G. Xie, and B.-T. Wang, Monolayer SnP_3: An excellent p-type thermoelectric material, Nanoscale **11**, 19923 (2019).

[57] B. Liu, Ni(111) defect-phonon scattering, 10.5281/zenodo .10155530 (2023).